Desalination and Water Treatment
www.deswater.com

doi: 10.5004/dwt.2018.23082

122 (2018) 339–350
August

Kinetic, isothermal and thermodynamic investigation on electrocoagulation of Congo red dye removal from synthetic wastewater using aluminium electrodes

M.S. Ramya Sankar[a], V. Sivasubramanian[a,*], E.V. Vidya Vijay[a], M. Jerold[b], J. Kanimozhi[a], P. Sinu[a], N. Shankar[a]

[a]*Department of Chemical Engineering, National Institute of Technology, Calicut, India 673601; emails: siva@nitc.ac.in (V. Sivasubramanian), ramya.msankar@gmail.com (M.S. Ramya Sankar), vidyavijayev@gmail.com (E.V. Vidya Vijay), jerold88@gmail.com (M. Jerold), kanimozhireddy@yahoo.co.in (J. Kanimozhi), sinumadhav@gmail.com (P. Sinu), shankar.nalinakshan@gmail.com (N. Shankar)*
[b]*Department of Biotechnology, National Institute of Technology, Warangal, Warangal 506 004, Telangana, India; email: jerold@nitw.ac.in*

Received 16 April 2018; Accepted 28 August 2018

ABSTRACT

The main objective of this study was the removal of an anionic bisazo dye from synthetic wastewater using electrocoagulation (EC) process. An electrochemical reactor was used with commercially available scrap aluminium sheets as electrodes (composition in weight %: aluminium, 48.71; carbon, 24.74; oxygen, 26.55). Literature suggests that most influencing factors of the process were identified as initial concentration, reaction time, initial pH, current density (CD), rotational speed and interelectrode distance. The pollutant removal performance was investigated over a wide range of initial concentration (10–100 ppm), reaction time (0–120 min), pH (3–11), CD (0–350 mA cm^{-2}), rotational speed (200–1,000 rpm) and of interelectrode distance (1–6 cm). The results showed that the removal efficiency of pollutants increases with increasing both EC residence time and direct current (DC) density. Higher removal efficiency was found at neutral to alkaline region pH of 7–9, interelectrode distance and speed of agitation has an inverse relationship to the response. Over 93% of removal efficiently was observed by conducting the EC treatment at a CD of 200 mA cm^{-2}, pH of 8, EC time of 60 min, interelectrode distance of 3.5 cm and agitation speed of 200 rpm. Moreover, the kinetic study demonstrated that the removal of such an azo dye follows the pseudo-second-order model with current-dependent parameters. The electrically formed by-products were analyzed by Fourier-transform infrared spectroscopy and scanning electron microscopy. The obtained results were compared with the raw dye used for the preparation of synthetic wastewater and confirmed that these are removed along with the aluminium hydroxides [1].

Keywords: Electrocoagulation; Congo red dye; SEM; FTIR

1. Introduction

Water dearth is one of the paramount current and future challenges faced by the humankind as the world population and water consumption rate is continuously increasing [2]. In view of this increasing need of water and stringent environmental policy adopted by industrialized countries demands efficient and eco-friendly method of water treatment [3,4]. Industries such as textiles, printing, paint, paper and pulp are the most polluting source of water bodies [5,6]. Industries of these kind and many more utilize dyes in order to colour their products and consume a large amount of water in processing and finishing stage. They are

* Corresponding author.

Presented at the 3rd International Conference on Recent Advancements in Chemical, Environmental and Energy Engineering, 15–16 February, Chennai, India, 2018.

often rich in colour, contains residue of reactive dyes and many toxic chemicals. A proper attention should be given before releasing these to the environment. In the present scenario, textile industries are the main consumers of dyes, and they produce a wide variety of dye effluents. Among different types of commercial dyes, azo dyes show very crucial and long-term impact on the environment [2,3,7,8].

When dyes react with water due to their complex structure that leads to certain serious impact such as chronic toxicity often leads to mutagenic and carcinogenic effects. More than 50% of the commercially available dyes can be classified into an azo group. These groups of compounds show complex chemical formula, toxic and poor biodegradability due to the presence of benzidine, naphthalene and other aromatic compounds [9].

To avoid the dangerous accumulation of these dyes they should be treated by proper methods before disposal. Conventionally the effluents were treated by chemical, physical and biological methods. Extensively used methods include adsorption, precipitation, chemical degradation, photodegradation, biodegradation, chemical coagulation and membrane processes. Due to the complex chemical and aromatic molecular structure and stability towards light the removal efficiency is limited. All these methods are not cost-effective and environment-friendly. As a result, an environment-friendly and cost-effective method has to be proposed for the efficient removal of dyes [4]. Recent researchers have demonstrated that electrochemistry offers an attractive alternative to overcome these problems [10]. These include the processes like electrocoagulation (EC); electrooxidation is very attractive for the decontamination of wastewater without the addition of any toxic chemicals. The electrochemical technique shows some promising approaches such as (i) prevention of pollution, (ii) versatility, (iii) environmental compatibility and (iv) cost-effectiveness [3,11,12].

EC is a process in which the in-situ generation of coagulants takes place. It accounts for the function and advantage of conventional coagulation, flotation and electrochemistry in water and wastewater industry. Al/Fe plates are normally used for EC process, the dissolution of the anode take places by applying a potential difference between the electrodes. When the sacrificial electrodes are immersed in the pollutant water, they give rise to the corresponding metal ions as follows [5,6]:

Anode:

$$Al_{(s)} + 3e^- \rightarrow Al^{3+} \quad (1)$$

Cathode:

$$2H^+ + 2e^- \rightarrow H_2 + OH^- \quad (2)$$

$$2H_2O + 2e^- \rightarrow H_2 + OH^- \quad (3)$$

Overall:

$$Al^{3+} + 3OH^- \rightarrow Al(OH)_{3(s)} \quad (4)$$

EC has been known for over a century, but was not found widely due to its high investment and operation cost. Meanwhile the demand for high-quality water and eco-friendly treatment methods leads to the application of EC in the water treatment field. EC equipment is very simple to operate, as no addition of chemicals, the sludge production is also very less, operated at short times. All the above are the main advantages of the process [10,13].

The main reagent involved in the process is 'electron' which is a clean reagent so these are much compatible with the environment. The electrochemically generated ions will undergo electrolysis near anode and produce active intermediates; they destabilize the colloidal particles which will aggregate and form flocs [10]. Compared with the traditional coagulation and flocculation methods, these can be used for removal of a wide spectrum of pollutants even in the colloidal range of particle size.

The EC process also finds applications for the treatment of real wastewater such as paper mill wastewater. The effluent collected from the industry having very high chemical oxygen demand (COD) value and the presence of lignin resists the application of biological wastewater, thus this can be overcome by EC process and found more than 85% removal efficiency with disc-type anode [11]. Adhoum et al. [14] investigated the applicability of EC for the treatment of electroplating wastewater with 94% of copper removal efficiency. Copper, zinc and chromium ions together with high COD were removed from electroplating industry [14]. From the industrial wastewater, the removal of copper, chromium and nickel with high removal efficiency from an electrochemical reactor with plate electrodes was investigated [15]. Rice mill wastewater treatment [16] and bilge water [11] are also the examples for real water application of EC.

Congo red dye is a benzene-based anionic diazo dye widely used in textile industries, and they cause chemico-azo stress on aquatic organisms even at a very small amount. Structure and characteristics of Congo red dye are shown in Table 1 for this work, the aluminium electrodes were used in the batch system and the removal efficiency was determined by varying different parameters [17,18].

2. Materials and methods

2.1. Dye solution preparation

This study concentrates on the removal of Congo red dye (Nice Chemicals, Kochi, Kerala, India, commercial grade with 70% purity) with molecular structure is shown in Fig. 1 and all other chemicals (with 98%) purity used without further purification. Required concentrations of dye were prepared by dissolving an appropriate amount of dye in Millipore water unit, pure lab option Q ELGA. The pH of the solution was adjusted using 1N H_2SO_4 and 1 N NaOH to a desirable value.

2.2. Electrodes used

Aluminium electrodes were used as both anode and cathode in the process of Congo red dye removal by EC. The aluminium electrodes used in this study are highly cost–effective. The commercial grade aluminium with a

Table 1
Properties of Congo red dye [8]

CA index name	1-Naphthalenesulfonic acid, 3,3,-[[1,1′-biphenyl]-4,4′-diylbis(2,1-diazenediyl)]bis[4 amino-, sodium salt (1:2)]
Molecular formula	$C_{32}H_{22}N_6Na_2O_6S_2$
Molecular weight	696.66 g mol^{-1}
Physical form	Brownish red powder
Molecular surface area	55,706 $Å^2$
Solubility	Soluble in water and ethanol; very slightly soluble in acetone; practically insoluble in ether and xylene
Melting point	>360°C
pH range	3.0–5.0
Colour	Blue (pH 3.0) to red (pH 5.0)
Absorption wavelength	497 nm

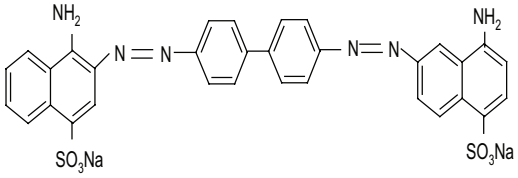

Fig. 1. The molecular structure of Congo red dye.

composition in wt% of aluminium: 48.71, carbon: 24.74, oxygen: 26.55. These attributes are not in the case of other studies which used aluminium as electrodes.

2.3. Experimental setup and procedure

EC involves many chemical and physical steps that use sacrificial electrodes to liberate the ions which act as the coagulants for the removal of pollutants [3]. Fig. 2 represents the experimental setup of the EC process. The EC setup consists of an electrochemical reactor (1,000 mL glass beaker), direct current power supply from which the connections to the electrodes are given and the electrodes were immersed in the solution which is to be treated. A good mass transfer was obtained by giving constant agitation by means of a magnetic stirrer. A suitable choice of electrode material was selected (aluminium) which in turn affects the cell voltage and liberates the coagulants. The electrode plates of dimensions 5 × 5 × 1 cm were hanged with an interelectrode distance of 3 cm. The passivation of electrodes takes place during the EC process so it is necessary to clean the electrodes. All experiments were carried out at room temperature.

The experiments were conducted using aluminium strips as electrode materials to remove the Congo red dye from simulated wastewater. Various operational parameters such as reaction/removal time, the initial concentration of dye, pH for the removal, the effect of current density (CD) and the rotational speed, interelectrode distance on the removal of Congo red were determined. After the EC process, the flocs formed were separated by letting the solution to settle. The supernatant collected was used to find out residual Congo red present in the solution. After each set of experiments, the electrodes were cleaned by scrubbing the surface and washed with dilute acid or alkali [19].

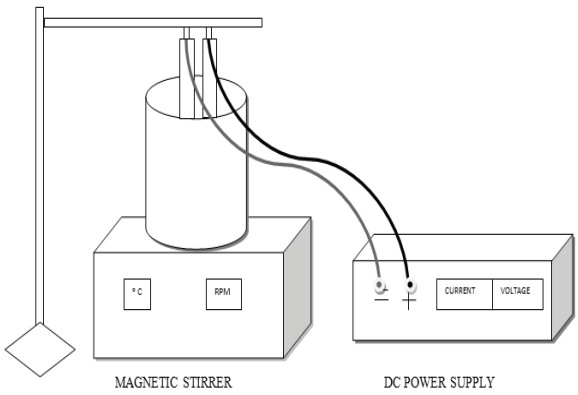

Fig. 2. Experimental setup of electrocoagulation.

2.4. Analytical procedure

Once the EC experiment is completed the pollutant from effluent was separated into two phases, pollutant-rich phase along with aluminium hydroxide coagulant and clear liquid. The clear liquid was analyzed with the help of double beam UV-visible spectrophotometer (Perkin Elmer Lambda 650, USA) at 497 nm (wavelength) [18]. The dye removal percentage was obtained as follows:

$$\% \text{ Removal} = \left(\frac{C_i - C_f}{C_i} \right) \times 100 \quad (5)$$

where C_i is the initial dye concentration and C_f is the final dye concentration of Congo red dye (mg L^{-1}).

The characterization studies of the pollutant-rich phase were conducted to obtain the surface morphology by means of scanning electron microscopy (SEM; JEOL Model JSM - 6390LV), Fourier-transform infrared spectroscopy (FTIR) (Thermospecific Agilent Cary 630 FTIR Spectrometry, India) helped to find out the involvement of functional groups in the flocs. Floc spectra were collected in the wavelength range of 500–4,000 cm^{-1}. And from the XRD patterns of the electrolysis by-products were compared with the dye before EC.

2.5. Kinetic, isotherms and thermodynamic modelling

2.5.1. Kinetic models

Kinetic studies have a very important role in determining the rate of reaction and order of the reaction, which further helps in the reactor design. Rate and order of reaction describes the rate of change in concentration of reactant per unit time [20–22]. The effects of CD, reaction time, initial dye concentration, initial pH, agitation speed and interelectrode distance on the removal efficiency were studied. The sample solution was withdrawn at particular time intervals and analyzed the residual dye content in the treated sample by UV-visible spectrophotometer. The electrode consumption was estimated according to Faraday's law and the amount of flocs generated was estimated stoichiometrically. The pollutants present in the solution were adsorbed into the flocs, so the pollutant removal can be modelled by the amount of dye coagulated at equilibrium Q_e mg g^{-1} has been found by the following equation:

$$Q_t = \frac{(C_i - C_t)V}{M} \tag{6}$$

where V is the solution volume (L), M is the weight of anode dissolved (g); C_0 and C_t are the initial and equilibrium concentrations of Congo red dye (mg L^{-1}), respectively [10].

2.5.1.1. Pseudo-first-order kinetic model A simple kinetic analysis of the process under the pseudo-first-order assumption is given by the following equation:

$$\frac{dQ}{dt} = K_1(Q_e - Q_t) \tag{7}$$

where Q_e and Q_t are the dye concentrations (mg g^{-1}) at equilibrium and at time t (min), respectively, k_1 is the adsorption rate constant (min^{-1}) and t is the contact time (min).

2.5.1.2. Pseudo-second-order kinetic model A pseudo-second-order kinetic model is based on equilibrium adsorption and it is expressed in Eq. (7).

2.5.2. Isotherm models

The equilibrium data from this study were described with different adsorption isotherm models, that is, Langmuir (1918), Freundlich (1906), Temkin and Dubinin–Radushkevich (1947) [13,18,23]. The acceptability and suitability of the isotherm equation to the equilibrium data were based on the values of the coefficient of determination R^2 estimated from linear regression of the least square fit.

2.5.2.1. Langmuir isotherm Langmuir isotherm equation is based on the following assumptions: (1) the entire surface for the adsorption has the same activity for adsorption, (2) there is no interaction between adsorbed molecules and (3) all the adsorption occurs by the same mechanism and the extent of adsorption is less than one complete monomolecular layer on the surface. Langmuir equation is given by Eq. (8) (Langmuir 1918):

$$Q_{eq} = \frac{Q_0 K_{LC_e}}{1 + K_L C_e} \tag{8}$$

where Q_0 is the maximum amount of the dye molecule per unit weight of the coagulant to form a complete monolayer on the surface, C_e (mg g^{-1}) is the concentration of the dye remaining in solution at equilibrium and b is equilibrium constant (dm^3 mg^{-1}). The shape of Langmuir isotherm can be used to predict whether a process is favourable or unfavourable in a batch adsorption process. The essential features of Langmuir isotherm can be expressed in terms of a dimensionless constant separation factor (R_L).

$$R_L = \frac{1}{1 + K_{LC_0}} \tag{9}$$

where C_0 is the initial concentration (mg L^{-1}) and K_L is the Langmuir equilibrium constant (L mg^{-1}).

2.5.2.2. Freundlich isotherm The Freundlich isotherm is an empirical equation based on sorption on a heterogeneous surface. It is assumed as stronger binding sites are occupied first and that the binding sites strength decreases as the rate at which the sites are occupied increases. It is commonly presented as follows:

$$Q_e = K_F \tag{10}$$

where K_F and n are the Freundlich constants related to the adsorption capacity and intensity of the sorbent, respectively.

2.5.3. Thermodynamic studies

The type of energy changes occurred in the adsorption process was explained by the thermodynamic parameters. In order to evaluate the adsorption process thermodynamic parameters such as change in standard enthalpy ($\Delta H°$), change in standard entropy ($\Delta S°$) and change in standard free energy ($\Delta G°$) were evaluated [18,21].

These values can be calculated using the following equation:

$$\ln K_d = \frac{\Delta S_0}{R} - \frac{\Delta H_0}{RT} \tag{11}$$

where K_d is the equilibrium constant obtained as $K_d = Q_e/C_e$ calculated at different temperatures. A linear plot of ln K_d vs. $1/T$ is obtained from which $\Delta S°$ and $\Delta H°$ can be calculated.

The positive values for standard enthalpy change indicate that the adsorption process is endothermic in nature and for negative values the process is in exothermic in nature. The positive values for entropy change indicate the increment in the randomness at solid solution interface. $\Delta G°$ can be calculated using Eq. (12). The negative values for $\Delta G°$ show the process is spontaneous [24].

$$\Delta G° = -RT \ln K_L \tag{12}$$

The activation energy is obtained from the plot of ln K_2 against $(\frac{1}{T})$ gives slope as $(\frac{-E_a}{RT})$.

The nature of adsorption process can be determined by the magnitude of activation energy E_a, by using the Arrhenius equation it can be determined either the process is physical or chemical. Physisorption process has the activation energy ranging from 5 to 40 kJ mol^{-1}. For chemisorption process, the activation energy is higher and ranging from 40 to 800 kJ mol^{-1} [13,18]. As shown in the following relationship, Arrhenius equation can be represented as follows:

$$\ln K_2 = \ln A - \frac{E_a}{RT} \tag{13}$$

where K_2 is the rate constant obtained from the pseudo-second-order kinetic model (g mg^{-1} h); A, the Arrhenius factor; E_a, the Arrhenius activation energy of adsorption (kJ mol^{-1}); R, the universal gas constant (8.314 J mol^{-1} K^{-1}); T, the absolute temperature (K).Therefore, a plot of ln K_2 against 1/T will yield the values of activation (E_a) from the slope of the graph, $\frac{-Ea}{R}$.

3. Result and discussion

EC involves many chemical and physical steps and this depends on material properties as well as various operational parameters. Here the subjected work deals with the optimization of parameters, characterization of by-products then kinetic, isothermal and thermodynamic studies. All the experiments were triplicated, and the percentage error was obtained on an average as 5 and error bars were plotted.

3.1. Optimization of operating parameters

3.1.1. Effect of initial concentration

Concentration of dye present in the effluent stream is in wide-range compositions. Fig. 3 shows the effect of concentration on removal efficiency, and it was studied by varying concentration from 1 to 100 ppm. Fig. 3 depicts as the concentration increases the removal efficiency decreases up to 20 ppm. This is most probably due to the amount of aluminum hydroxides formed will be insufficient, as the concentartion increases at constant CD.(decolrization of reactive blue). A very interesting phenomenon observed after 20 ppm was that the removal efficiency started increasing, this is due to a crucial role played by conductivity. As the concentration of dye increases the conductivity also increases. Conductivity is the main parameter which determines the efficiency of EC process. The reaction conditions were kept constant at a time of 120 min, of 7 pH, CD 200 mA cm^{-2}, agitation speed of 200 rpm and interelectrode distance of 3 cm. The plots are single, smooth and continous leading to saturation suggesting the possible monolayer coverage. Similar results were dissucced by Vasudevan et al. [10], Adeogun and Balakrishnan [8], Manoj Babu and Goel [25], and Daneshvar et al. [26].

3.1.2. Effect of reaction time

Another most influencing factor on the process of EC is reaction time. Fig. 4 shows that the effect of reaction time on the removal efficiency was studied from 15 to 120 min at an initial concentration of 40 ppm, pH 7 and CD of 200 mA cm^{-2}, interelectrode distance of 3.5 cm, rotational speed at 200 rpm and time of 60 min were obtained as optimum values.

Dye removal efficiency reached from 40% to 98% at a time of 15–120 min. As the reaction time increases the time of mixing and the reaction increased, after 60 min the removal efficiency was found as constant [3,16]. Rest of the experiments were conducted on the optimized time (60 min).

3.1.3. Effect of pH

pH is the key parameter in the EC process. The freshly formed cation hydroxides will destabilize the colloidal particles in the solution. When pH is between 4 and 9 Al^{3+}, OH^- ions generated by the electrodes react to form various monomeric and polymeric species such as $Al(OH)^+_2$, $Al(OH)^-_2$ and $Al_6(OH)_{15}^{3+}$, $Al_7(OH)_{17}^{4+}$ etc., and the species transform into insoluble amorphous $Al(OH)_3$ solids through complex

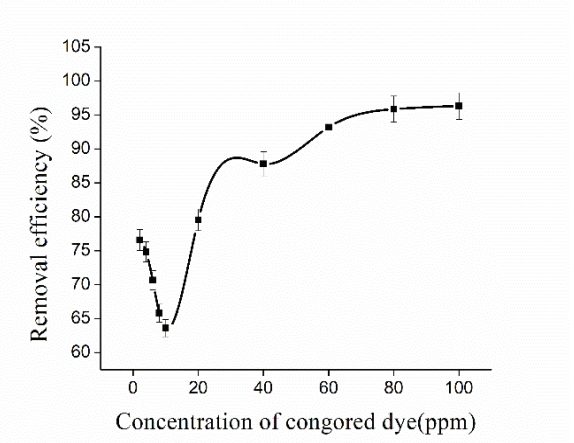

Fig. 3. Effect of concentration on removal efficiency.

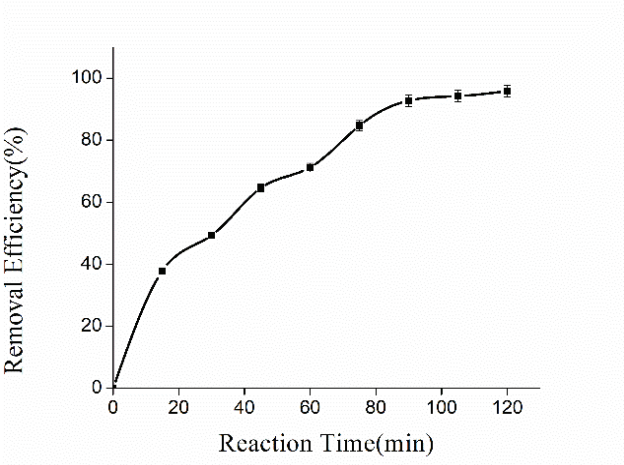

Fig. 4. Effect of time on the removal efficiency.

kinetic precipitation or polymerization [3,9,11]. The effective coagulant species formation was observed at neutral to the slightly acidic region. In the highly basic regions $(AlOH)^{4-}$ is formed and it shows very poor coagulating performance towards the anionic pollutant species [11]. To evaluate the effect of pH on the removal efficiency the experiments were performed using 40 ppm solutions with initial pH varying from 3 to 12 and optimum was found at 8. All other conditions were kept at 60 min time, the CD of 200 mA cm^{-2}, interelectrode distance of 3.5 cm and rotational speed as 200 rpm. The results were shown in Fig. 5. In this study, the results agree well with the results present in the literature and maximum removal was found at neutral to alkaline region [4,10,11].

3.1.4. Effect of CD

It has been established that the applied CD has considerable effect on the performance of an EC reactor [11]. The current applied per unit area determines the electro coagulant dosage rate, which indicates that the efficiency of removal depends on the availability of binding sites. In Fig. 6 it depicts that as the CD is increased more Al dissolves from anode into solution and also small bubbles of H generated according to Faraday's law which overall results in the availability of Al(OH) hydroxyl polymers for the adsorption of dye molecules, thus the removal efficiency also increases [3,19,27,28]. It was observed that as the CD varied from 70 to 335 mA cm^{-2}, the removal efficiency was also increased from 47% to 96%. The experiments were carried out under the following conditions reaction time of 60 min, pH of 8, an interelectrode distance of 3.5 cm and Al as an electrode.

As the EC process proceeds, the solution becomes more turbid and, as a final result, the removal efficiency and consequently the flocculation rates also increase [1].

3.1.5. Effect of rotational speed

The effect of rotational speed on the removal efficiency was investigated from 200 to 1,200 rpm, and the results are depicted in Fig. 7. As the stirring speed increases the removal efficiency decreased. In the EC process metal hydroxides stabilize the dispersed particles. Thus the electrostatic repulsion between the particles will reduce. Agitation plays a crucial role in bringing the particles together to a point where Van der Waals force of attraction becomes predominant and provides uniform bulk distribution of generated ions [29,30]. The experiments were conducted at 40 ppm initial concentration, initial pH of 8, the CD of 200 mA cm^{-2} and electrode spacing of 3.5 cm, the maximum removal was found at 200 rpm. The removal efficiency of 98% at 200 rpm was decreased to 40% at 1,200 rpm due to the degradation of floc by collisions between them at higher agitation speed.

3.1.6. Effect of interelectrode distance

The effect of interelectrode distance was investigated with the aim of determining the removal efficiency of pollutant present. The electrode spacing increases as the percent removal was found to be decreased. A similar behavior was already observed by Aswathy et al. [11] during the treatment of Bling water by EC. As the interelectrode spacing is increased the resistance between the electrodes also increases, so more initial voltage is needed to reach the same CD and coagulant dosage [3,28].

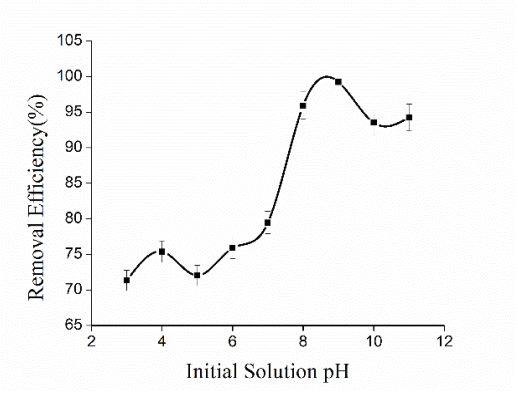

Fig. 5. Effect of pH on removal efficiency.

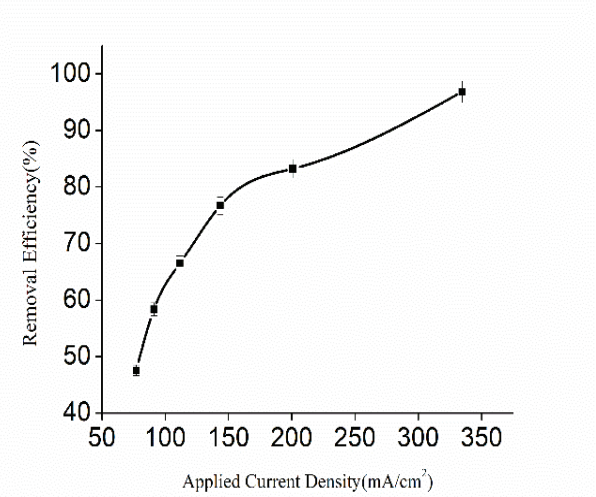

Fig. 6. Effect of CD on removal efficiency.

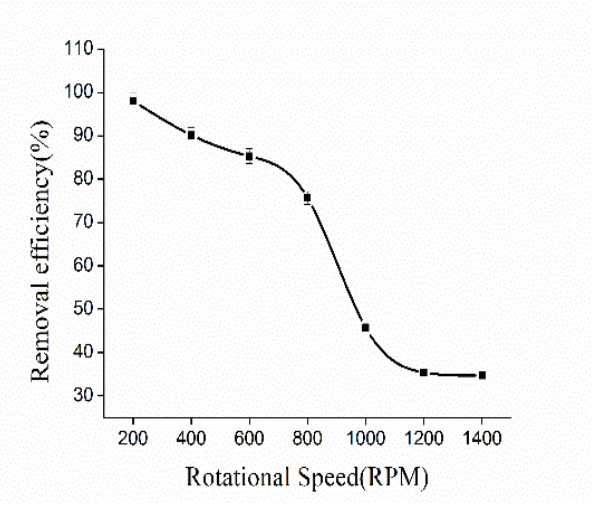

Fig. 7. Effect of rotational speed on removal efficiency.

As the electrode spacing increased from 2 to 6 the removal efficiency was found to be decreased from 99% to 65%, at 90 min electrolysis time, of CD 200 mA cm^{-2} and of 8 pH is shown in Fig. 8. The electrical conductivity was directly proportional to the distance between the two electrodes, the electrode spacing increased the resistance between the electrodes as well as the power consumption for the removal also increases.

3.2. Material characterization

3.2.1. Scanning electron microscopy

3.2.1.1. SEM/EDAX of electrodes SEM images of commercial grade aluminium electrodes before and after EC process of Congo red dye electrolytes were obtained to analyze the surface texture. Fig. 9(a) shows the fresh aluminium electrode prior to the EC process; the surface was found to be uniform.

Fig. 9(b) shows SEM image of anode after several cycles of EC experiments. The electrode surface is now found to be rough with a number of dents and pores. These dents are formed around the active sites with the dissolution of aluminium electrodes which are then formed into the aluminium hydroxides. The formation of large number of pores attributed to the result of the anode material consumption and the oxygen formation [1,6,28]. Similar behaviours were obtained by the Elabbas et al. [28] and Hu et al. [6] for the removal of tannery wastewater and Humic Acid removal respectively.

The energy dispersive analysis of X-ray was used to analyze the elemental constitution of electrode before and after the EC experiments were studied. Figs. 10(a) and (b) show the energy dispersive x-ray spectroscopy images of anode before and after EC process, respectively. The results were observed as the aluminium composition is steeply decreased from 48.71 wt% to 27.51 wt% and the carbon wt% was increased from 24.74 wt% to 43.72 wt%. The above mentioned results show the dissolution of anode materials and they are converted into coagulant forms.

3.2.1.2. SEM of Congo red dye before and after (dye loaded with flocs) EC process Fig. 11 illustrates the SEM analysis of Congo red dye before and after EC process. Fig. 11(a) shows the surface morphology of dye before treatment, fine and less dense-powdered particles [29,31]. Fig. 11(b) shows the dye-loaded flocs, small flakes over the surface which are the characteristic images for aluminium hydroxides. Small flakes along with the dye after EC process images are shown in Fig. 11. It is concluded that the dyes are getting removed from the solution with aluminium hydroxide particles which are generated in situ by passing electricity.

The surface of the flocs has many pores which are covered with aluminium hydroxide particles which are visible in the form of small flakes on the surface.

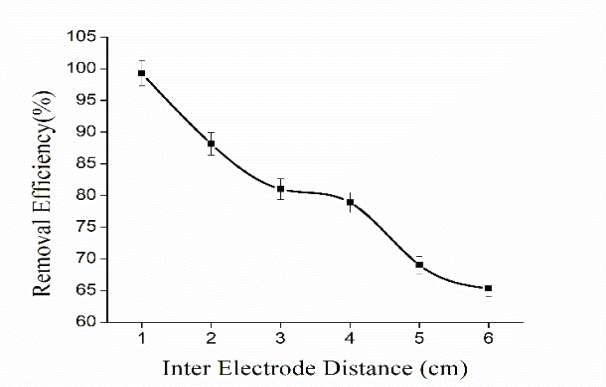

Fig. 8. Effect of interelectrode distance on removal efficiency.

3.2.2. Fourier-transform infrared spectroscopy

FTIR was used to determine the chemical functionalities of a material by passing an Infrared beam through which an absorption spectrum of defined wavenumber and fingerprint of the sample showing stretching, contraction and the bending of chemical bonds is obtained. It depends on the interaction of infrared radiations with chemical functionalities of a sample. It is easy to perceive the alterations in peaks before and after the experiments [31,32]. FTIR spectrum of dye and dye aluminium electrode by-product is shown in Fig. 12, which is measured in the frequency range of 1,500–2,000 cm^{-1}.

The characteristic peaks of Congo red dye with functional groups and vibrational frequency are assigned as follows: 1,259, 1,068 and 1,016 for SO_3H; 1,500–2,000 cm^{-1}

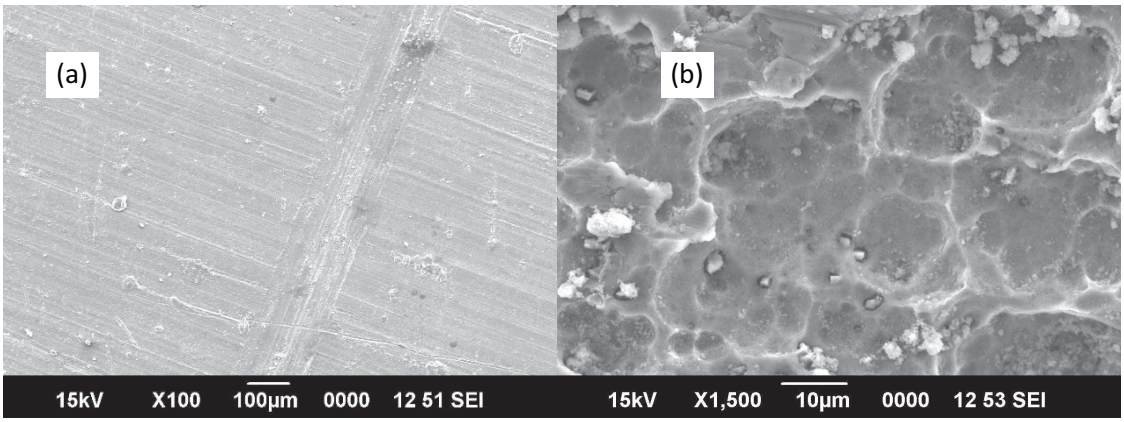

Fig. 9. SEM image of anode (a) before and (b) after electrocoagulation.

corresponding to N≡N; and 1,445 for an aromatic ring [16]. From aluminium electrode by-product OH stretching, hydroxyl bending and Al–OH bending are observed at 3,452, 1,638 and 400–500 cm^{-1}, respectively. A strong S=O stretching at 1,068 cm^{-1} and aromatic in plane stretching at 1,445 cm^{-1} are also found in the by-products of EC [11].

In the absorption peak the strong sulfonic acid group, azo group, and characteristic Al–OH are observed. The analysis of the by-products indicated that the chromophoric groups were destructed and the dye molecules were broken down into small particles and were removed along aluminium hydroxide particles. These results indicated the degradability of dyes [10]. The broadening of peaks is attributed to the dye molecules conjugation with the aluminium particles [24].

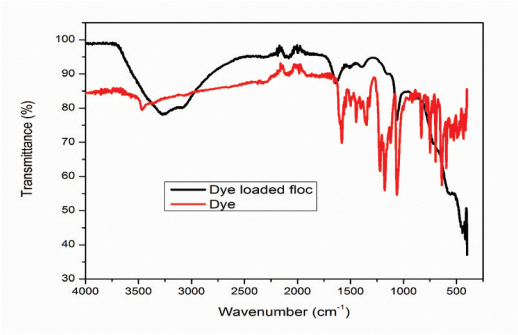

Fig. 12. FTIR of Congo red dye before EC and after EC.

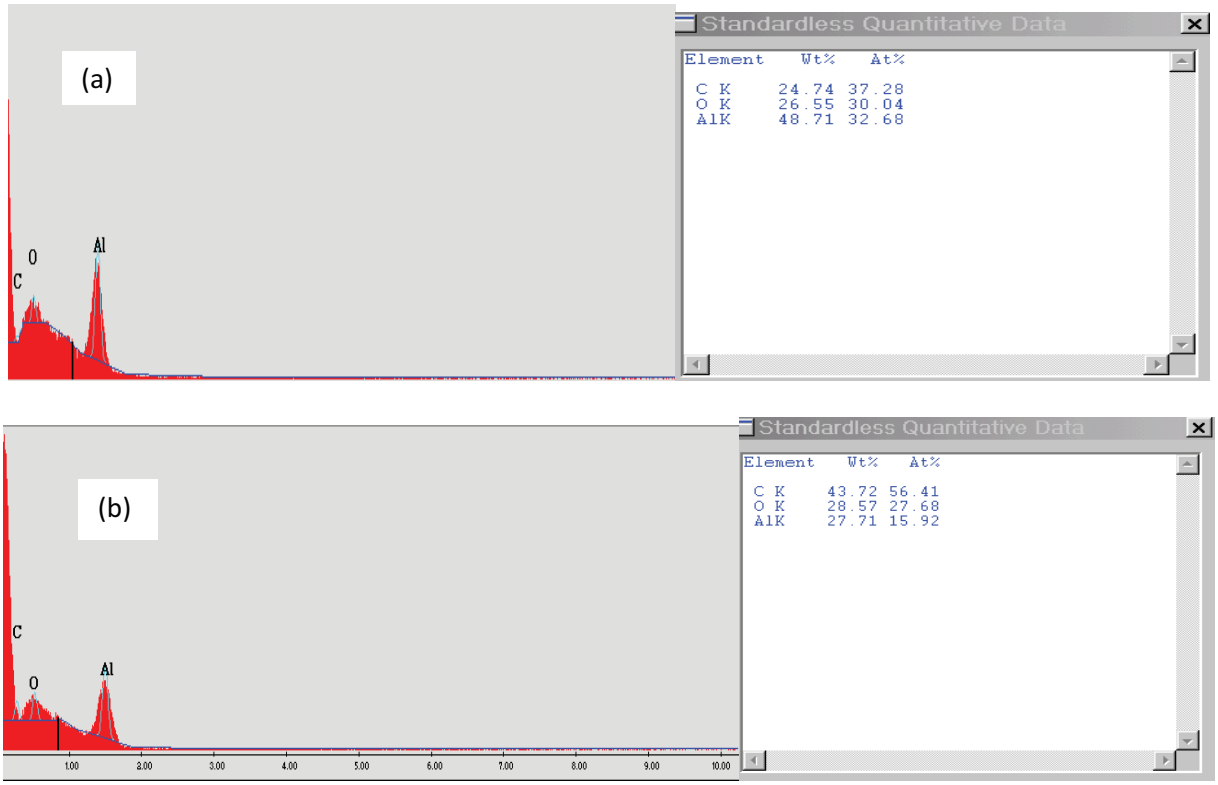

Fig. 10 The energy dispersive analysis of aluminium electrode (anode) (a) before and (b) after EC process.

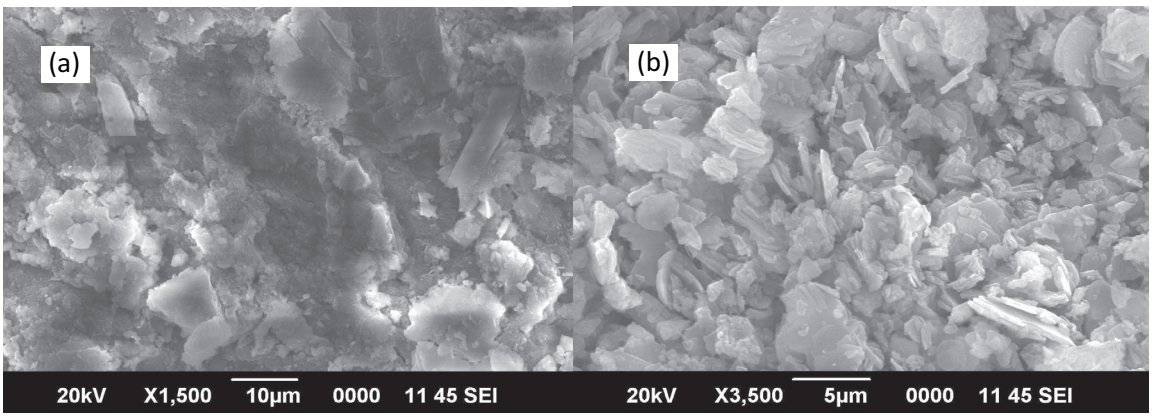

Fig. 11. Congo red dye (a) before EC and (b) dye-loaded floc.

3.3. Kinetic, isothermal and thermodynamic modelling

3.3.1. Kinetic models

Kinetic behavior of the process has been studied to attempt to learn about the adsorption kinetics and the rate-controlling steps including mass transfer and chemical reaction steps. The plots of two distinct kinetic models used to explain the kinetic behavior of the process are pseudo-first-order kinetic model and pseudo-second-order kinetic model.

3.3.1.1. Pseudo-first-order kinetic model Pseudo-first-order kinetic model kinetic data were analyzed by Lagergran rate equation. The linearized form of the pseudo-first-order rate equation was given as follows [18]:

$$\ln\left(Q_e - Q_t\right) = \ln Q_e - \frac{K_1 t}{2.303} \tag{14}$$

where Q_e and Q_t are the amount of Congo red dye adsorbed on the EC products at equilibrium (mg g^{-1}) and at time t, respectively, and K_1 (min) is the calculated rate constant of adsorption. The experimental data were analyzed with the pseudo-first-order model as shown in Fig. 13(a) and Table 2. From the plot of $\ln(Q_e - Q_t)$ versus the values of K_1, and Q_e can be determined as the slope and intercept of the plot respectively. Results show that experimental data did not completely follow a liner plot, the correlation coefficient was low and the calculated as well as the experimental values of Q_e are not matching each other. Hence, the reaction could not be categorized as the pseudo-first-order kinetic model [21].

3.3.1.2. Pseudo-second-order kinetic model The linearized form of the pseudo-second-order equation was represented as follows [11,24]:

$$\frac{t}{Q_t} = \frac{1}{K_2 Q_{e^2}} + \frac{t}{Q_e} \tag{15}$$

where K_2 is the second-order adsorption rate constant (min^{-1}) and Q_e is the adsorption capacity calculated by the pseudo-second-order kinetic model (μg g^{-1}). Rate constant parameters and Q_e values for different initial dye concentration is shown in Fig. 13(a) and Table 2. The Q_e and K_2 can be calculated from the slope and intercept of plot of t/Q_t vs. t. From Fig. 13(b) and Table 2, the plots were found to be linear with extremely high correlation coefficients. Besides, the theoretical values $Q_{e\,Cal}$ were in good agreement with the experimental values $Q_{e\,Exp}$ at all initial concentrations studied. It suggested that the pseudo-second-order model could be applied suitably to explain the adsorption of Congo red dye in EC process.

A similar kind of studies was reported by Song et al. [13] and Vasudevan et al. [22]; they also observed the reaction kinetics to be second order.

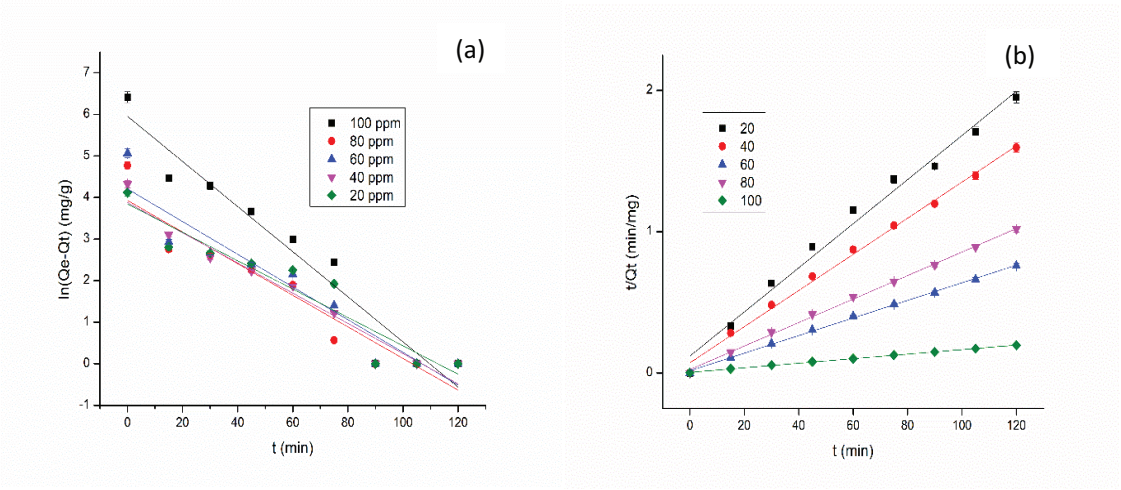

Fig. 13. Kinetics of electrocoagulation removal of Congo red dye: (a) pseudo first order and (b) pseudo second order.

Table 2
(a) Pseudo-first-order and (b) pseudo-second order rate constant parameters and Q_e values for different initial dye concentration

C_0	K_1	$Q_{e\,Exp}$	$Q_{e\,Cal}$	R^2	$Q_{e\,Exp}$	$Q_{e\,Cal}$	K_2	R^2
100	–0.124	609.341	384.710	0.929	61.518	64.1025641	0.0020	0.986
80	–0.087	117.887	50.857	0.889	75.189	78.125	0.0022	0.995
60	–0.090	158.155	67.139	0.892	117.887	120.481	0.0028	0.998
40	–0.08369	75.189	48.374	0.942	158.155	161.290	0.0024	0.998
20	–0.07858	61.518	46.712	0.886	609.341	625	0.0005	0.998

3.3.2. Isothermal model

3.3.2.1. Adsorption isotherms To perform the adsorption isotherms studies the equilibrium data were fitted to the Langmuir and Freundlich models. The Langmuir isotherm model assumed monolayer deposition of adsorbate on homogenous adsorbent surface.

The linearized form of Langmuir isotherm model was given as follows:

$$\frac{C_e}{Q_e} = \frac{1}{q_0 K_L} + \frac{C_e}{q_0} \tag{16}$$

where C_e (mg L^{-1}) is the equilibrium concentration of Congo red dye; Q_e (mg g^{-1}) is the amount of dye adsorbed at equilibrium; K_L (L mg^{-1}) is the equilibrium adsorption constant which is associated to the affinity of the binding sites; and Q_{max} (mg g^{-1}) is the Langmuir constant representing maximum monolayer adsorption capacity. The prominent feature of the Langmuir isotherm could be expressed by means of a separation factor or equilibrium parameter R_L, which was calculated by the following equation [13]:

$$R_L = \frac{1}{(1 + K_L C_0)} \tag{17}$$

where K_L (L mg^{-1}) is the Langmuir constant and C_0 (mg L^{-1}) is the maximum solute concentration. R_L values between 0 and 1 indicate that the adsorption process was favourable.

Experimental data were plotted as C_e/Q_e vs. C_e and shown in Fig. 14(a), and the values of Q_{max}, R_L, K_L, and R^2 are listed in Table 3(a).

3.3.2.2. Freundlich isotherm model To account the surface heterogeneity and distribution of the active adsorption sites lead to the possibility of multilayer formation, the mathematical expression of the Freundlich model was given by the following equation:

$$\ln Q_e = \ln K_f + n \ln C_e \tag{18}$$

where K_f (mg g^{-1}) and n are the constants that account for adsorption capacity of the adsorbent and the adsorption intensity. From Fig. 14(b) the K_f and $\frac{1}{n}$ values were found.

The pertinent of the two isotherm equations was compared by the correlation coefficient (R^2). From Table 3, the values of correlation coefficient (R^2) of the Langmuir model were found higher than that of the Freundlich model. Thus the Langmuir model provided a better fit than Freundlich model in the considered temperature range. Results indicated that Langmuir model could well describe the equilibrium isotherms. It could be concluded that the adsorption of Congo red dye in EC process serves monolayer adsorption [24].

3.3.3. Thermodynamic modelling

3.3.3.1. Adsorption thermodynamics studies The thermodynamic parameters ($\Delta G°$, $\Delta H°$, $\Delta S°$) were calculated from the following equations:

$$\ln K_d = \frac{\Delta S°}{R} - \frac{\Delta H°}{RT} \tag{19}$$

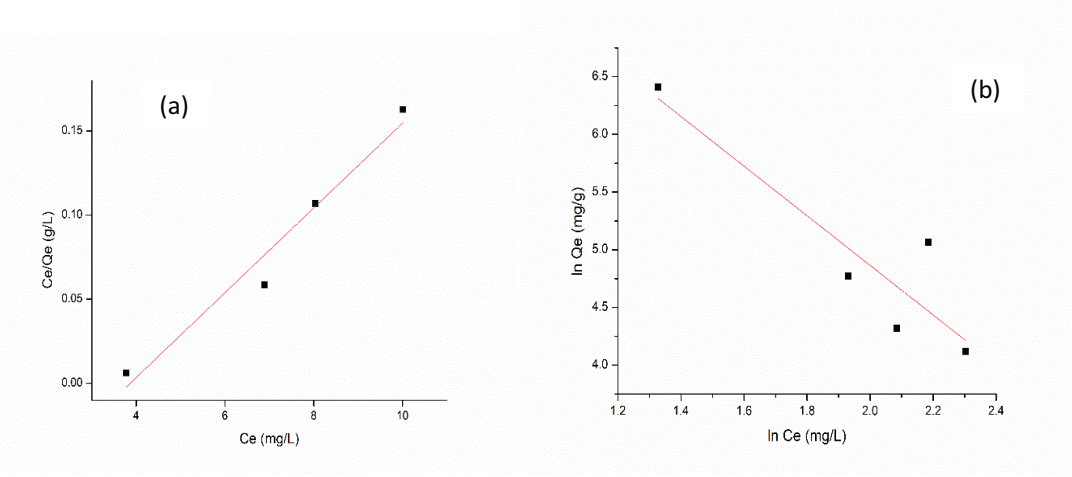

Fig. 14. Isothermal fits for electrocoagulation removal of Congo red dye: (a) Langmuir and (b) Freundlich.

Table 3
(a) Langmuir and (b) Freundlich isotherms for the removal of bromophenol Congo red dye

Langmuir				Freundlich		
Q_{max}	K_L	R_L	R^2	K_f	1/n	R^2
39.68253968	–0.0024	1.009320458	0.9661	9542.39	–0.465	0.7686

where $\Delta G°$ (kJ mol^{-1}) is the standard free energy change, K_d is the distribution coefficient, R is the universal gas constant (8.314 J (mol·K)$^{-1}$ and T is the temperature (K). The enthalpy change ($\Delta H°$) and entropy ($\Delta S°$) were calculated from the slope and intercept of the plot of ln K_d vs. 1/T as shown in Fig. 15. The thermodynamics constants obtained from the plot were given in Table 4. As shown in Table 4, the values of $\Delta G°$ were negative, indicating that the removal of Congo red dye by EC process was spontaneous and thermodynamically favourable. The positive values of $\Delta H°$ implied that the adsorption process was endothermic in nature. The positive values of $\Delta S°$ confirmed the increased randomness of the solution interface during the adsorption Congo red dye [17,24].

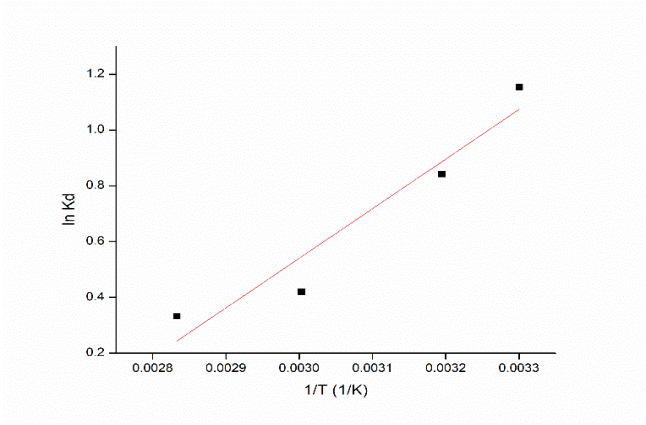

Fig. 15. Plot of ln K_d vs. 1/T for estimation of thermodynamic parameters for the electrocoagulation removal of Congo red dye.

Table 4
Thermodynamic parameters for the removal of dye

Temperature (°K)	ln K_d	ΔH	ΔS	ΔG	R^2
293	1.154	1,777.7	–4.7927	–1,726.010	0.9628
303	0.842			–2,907.504	
313	0.420			–2,191.694	
333	0.332			–1,164.397	

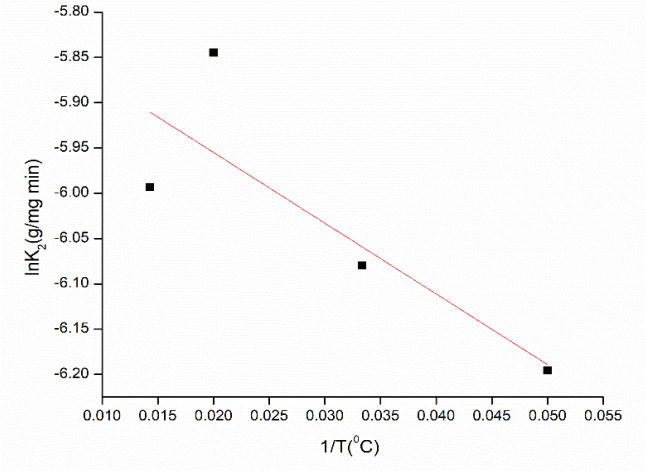

Fig. 16. Plot of ln K_2 vs. 1/T for estimation of thermodynamic parameters for the electrocoagulation removal of Congo red dye.

Furthermore, because the values of E_a obtained from the Fig. 16 of ln K_2 vs. 1/T is 64.9215 kJ mol^{-1}, which fall in the energy range of 80 to 800 kJ mol^{-1}, it confirms that the adsorption process was chemisorption.

4. Conclusion

EC is an effective option that can be chosen to treat toxic effluent than conventional chemical coagulation method. This study revealed the feasibility of the same in the removal of Congo red dye using a scrap aluminium sheet as the electrode. The process water was found to be dependent on the factors such as reaction time, pH, CD and rotational speed. The removal efficiency of 93% was observed at optimum conditions of 60 min of reaction time, pH of 8, the CD of 200 mA cm^{-2} and a rotational speed of 200 rpm.

The by-products of EC product were analyzed using SEM, FTIR which confirmed the removal of Congo red dye along with the freshly produced aluminium hydroxide coagulant. The reaction kinetics was studied by two different models and best fitted with pseudo-second-order kinetics. The adsorption isotherm was best fitted with Langmuir isotherm models, and the thermodynamic aspects of the process can be conclude as they are in spontaneous in nature ($\Delta G°$ is negative), endothermic ($\Delta H°$) as well as it shows an increment in the randomness at solid solution interface ($\Delta S°$).

Symbols

C_e	—	Equilibrium concentration of Congo red dye, mg L^{-1}
C_f	—	Final concentration of Congo red dye, mg L^{-1}
C_i	—	Initial concentration of Congo red dye, mg L^{-1}
F	—	Faraday's constant, C mol^{-1}
I	—	Current, A
K	—	Kinetic reaction rate constant
K_d	—	Distribution coefficient
K_F	—	Freundlich constant
K_L	—	Langmuir equilibrium constant, L mg^{-1}
M	—	Molecular weight of anode
Q_e	—	Amount of dye coagulated at equilibrium, mg g^{-1}
R	—	Universal gas constant, 8.314 J (mol·K)$^{-1}$
R^2	—	Root mean square value
R_L	—	Separation factor
t	—	Time, s
V	—	Volume of Congo red dye solution, mL
W	—	Weight of anode dissolved during the process, g
Z	—	Number of electrons involved in the redox reactions
$\Delta G°$	—	Standard free energy change, kJ mol^{-1}
$\Delta H°$	—	Standard enthalpy change, kJ mol^{-1}
$\Delta S°$	—	Standard entropy change, kJ mol^{-1}

References

[1] J.A.G. Gomes, P. Daida, M. Kesmez, M. Weir, H. Moreno, J.R. Parga, G. Irwin, H. McWhinney, T. Grady, E. Peterson, D.L. Cocke, Arsenic removal by electrocoagulation using combined Al-Fe electrode system and characterization of products, J. Hazard. Mater. 139 (2007) 220–231.

[2] D.T. Moussa, M.H. El-Naas, M. Nasser, M.J. Al-Marri, A comprehensive review of electrocoagulation for water treatment: potentials and challenges, J. Environ. Manage., 186 (2017) 24–41.
[3] E.S.Z. El-Ashtoukhy, A.A. Mobarak, Y.O. Fouad, Decolourization of reactive blue 19 dye effluents by electrocoagulation in a batch recycle new electrochemical reactor, Int. J. Electrochem. Sci., 11 (2016) 1883–1897.
[4] J. Vidal, L. Villegas, J.M. Peralta-Hernández, R. Salazar González, Removal of Acid Black 194 dye from water by electrocoagulation with aluminum anode, J. Environ. Sci. Health Part A Toxic/Hazard. Subst. Environ. Eng., 51 (2016) 289–296.
[5] Z. Zaroual, M. Azzi, N. Saib, E. Chainet, Contribution to the study of electrocoagulation mechanism in basic textile effluent, J. Hazard. Mater., 131 (2006) 73–78.
[6] C. Hu, J. Sun, S. Wang, R. Liu, H. Liu, J. Qu, Enhanced efficiency in HA removal by electrocoagulation through optimizing flocs properties: role of current density and pH, Sep. Purif. Technol., 175 (2017) 248–254.
[7] K. Sarath, R. Gandhimathi, S.T. Ramesh, P.V. Nidheesh, Removal of reactive magenta-MB from aqueous solution by persulphate-based advanced oxidation process, Desal. Wat. Treat., 57 (2016) 11872–11878.
[8] A.I. Adeogun, R.B. Balakrishnan, Electrocoagulation removal of anthraquinone dye Alizarin Red S from aqueous solution using aluminum electrodes: kinetics, isothermal and thermodynamics studies, J. Electrochem. Sci. Eng., 6 (2016) 199–213.
[9] S.S. Ma, Y. gang Zhang, Electrolytic removal of alizarin red S by Fe/Al composite hydrogel electrode for electrocoagulation toward a new wastewater treatment, Environ. Sci. Pollut. Res., 23 (2016) 22771–22782.
[10] S. Vasudevan, J. Lakshmi, J. Jayaraj, G. Sozhan, Remediation of phosphate-contaminated water by electrocoagulation with aluminium, aluminium alloy and mild steel anodes, J. Hazard. Mater., 164 (2009) 1480–1486.
[11] P. Aswathy, R. Gandhimathi, S.T. Ramesh, P.V. Nidheesh, Removal of organics from bilge water by batch electrocoagulation process, Sep. Purif. Technol., 159 (2016) 108–115.
[12] B.Z. Can, R. Boncukcuoğlu, A.E. Yılmaz, B.A. Fil, Arsenic and boron removal by electrocoagulation with aluminum electrodes, Arabian J. Sci. Eng., 41 (2016) 2229–2237.
[13] P. Song, Z. Yang, G. Zeng, X. Yang, H. Xu, J. Huang, L. Wang, Optimization, kinetics, isotherms, and thermodynamics studies of antimony removal in electrocoagulation process, Water Air Soil Pollut., 226 (2015) 380.
[14] N. Adhoum, L. Monser, N. Bellakhal, J.E. Belgaied, Treatment of electroplating wastewater containing Cu^{2+}, $Zn^{2+}$and Cr(VI) by electrocoagulation, J. Hazard. Mater., 112 (2004) 207–213.
[15] M. Hunsom, K. Pruksathorn, S. Damronglerd, H. Vergnes, P. Duverneuil, Electrochemical treatment of heavy metals (Cu^{2+}, Cr^{6+}, Ni^{2+}) from industrial effluent and modeling of copper reduction, Water Res., 39 (2005) 610–616.
[16] M. Thite, P.K. Chaudhari, Electrocoagulation of waste water and treatment of rice mill waste water: a review, 4 (2015) 233–239.
[17] M. Shafiqul Alam, Removal of Congo Red dye from industrial wastewater by untreated sawdust, Am. J. Environ. Prot., 4 (2015) 207.
[18] A.T. Ojedokun, O.S. Bello, Kinetic modeling of liquid-phase adsorption of Congo red dye using guava leaf-based activated carbon, Appl. Water Sci., 7 (2017) 1965–1977.
[19] R. Khosravi, S. Hazrati, M. Fazlzadeh, Decolorization of AR18 dye solution by electrocoagulation: sludge production and electrode loss in different current densities, Desal. Wat. Treat., 57 (2016) 14656–14664.
[20] N. Ghalwa M.A., Removal of imidacloprid pesticide by electrocoagulation process using iron and aluminum electrodes, J. Environ. Anal. Chem., 02 (2015). doi: 10.4172/2380-2391.1000154.
[21] I.A.W. Tan, A.L. Ahmad, B.H. Hameed, Adsorption isotherms, kinetics, thermodynamics and desorption studies of 2,4,6-trichlorophenol on oil palm empty fruit bunch-based activated carbon, J. Hazard. Mater., 164 (2009) 473–482.
[22] S. Vasudevan, J. Lakshmi, G. Sozhan, Studies on the removal of iron from drinking water by electrocoagulation – a clean process, Clean Soil Air Water, 37 (2009) 45–51.
[23] F. Fu, Q. Wang, Removal of heavy metal ions from wastewaters: a review, J. Environ. Manage., 92 (2011) 407–418.
[24] A.I. Adeogun, R.B. Balakrishnan, Kinetics, isothermal and thermodynamics studies of electrocoagulation removal of basic dye rhodamine B from aqueous solution using steel electrodes, Appl. Water Sci., 7 (2017) 1711–1723.
[25] J. Manoj Babu, S. Goel, Defluoridation of drinking water in batch and continuous-flow electrocoagulation systems, Pollut. Res., 32 (2013) 727–736.
[26] N. Daneshvar, A. Oladegaragoze, N. Djafarzadeh, Decolorization of basic dye solutions by electrocoagulation: an investigation of the effect of operational parameters, J. Hazard. Mater., 129 (2006) 116–122.
[27] J. Lu, Z.R. Wang, Y.L. Liu, Q. Tang, Removal of Cr ions from aqueous solution using batch electrocoagulation: Cr removal mechanism and utilization rate of in situ generated metal ions, Process Saf. Environ. Prot., 104 (2016) 436–443.
[28] S. Elabbas, N. Ouazzani, L. Mandi, F. Berrekhis, M. Perdicakis, S. Pontvianne, M.N. Pons, F. Lapicque, J.P. Leclerc, Treatment of highly concentrated tannery wastewater using electrocoagulation: Influence of the quality of aluminium used for the electrode, J. Hazard. Mater., 319 (2016) 69–77.
[29] U. Tezcan Un, S. Topal, F. Ates, Electrocoagulation of tissue paper wastewater and an evaluation of sludge for pyrolysis, Desal. Wat. Treat., 57 (2016) 28724–28733.
[30] C.P. Nanseu-Njiki, S.R. Tchamango, P.C. Ngom, A. Darchen, E. Ngameni, Mercury(II) removal from water by electrocoagulation using aluminium and iron electrodes, J. Hazard. Mater., 168 (2009) 1430–1436.
[31] R. Kanthapazham, C. Ayyavu, D. Mahendiradas, Removal of Pb^{2+}, Ni^{2+} and Cd^{2+} ions in aqueous media using functionalized MWCNT wrapped polypyrrole nanocomposite, Desal. Wat. Treat., 57 (2016) 16871–16885.
[32] P. Giridhar, B. Weidenfeller, S.Z. El Abedin, F. Endres, Electrodeposition of iron and iron–aluminium alloys in an ionic liquid and their magnetic properties, Phys. Chem. Chem. Phys., 16 (2014) 9317.